Journal of Sound and Vibration 416 (2018) 192–212

Contents lists available at ScienceDirect

Journal of Sound and Vibration

journal homepage: www.elsevier.com/locate/jsvi

Experimental feedback linearisation of a vibrating system with a non-smooth nonlinearity

D. Lisitano [a], S. Jiffri [b], E. Bonisoli [c], J.E. Mottershead [b,*]

[a] Department of Management Production Engineering, Politecnico di Torino, Torino, 10129, Italy
[b] School of Engineering, University of Liverpool, Liverpool, L69 3GH, United Kingdom
[c] Department of Mechanical and Aerospace Engineering, Politecnico di Torino, Torino, 10129, Italy

ARTICLE INFO

Article history:
Received 13 July 2017
Received in revised form 22 November 2017
Accepted 24 November 2017
Available online 22 December 2017

Keywords:
Non-smooth systems
Active control
Feedback linearisation

ABSTRACT

Input-output partial feedback linearisation is demonstrated experimentally for the first time on a system with non-smooth nonlinearity, a laboratory three degrees of freedom lumped mass system with a piecewise-linear spring. The output degree of freedom is located away from the nonlinearity so that the partial feedback linearisation possesses nonlinear internal dynamics. The dynamic behaviour of the linearised part is specified by eigenvalue assignment and an investigation of the zero dynamics is carried out to confirm stability of the overall system. A tuned numerical model is developed for use in the controller and to produce numerical outputs for comparison with experimental closed-loop results. A new limitation of the feedback linearisation method is discovered in the case of lumped mass systems – that the input and output must share the same degrees of freedom.

1. Introduction

The growing demand for increased performance of mechanical and aerospace systems with reduced weight and fewer emissions leads to research initiatives that aim to exploit the characteristics of nonlinear systems. While the control of linear systems is well understood, most engineering systems behave nonlinearly, at least to some degree, and require the application of a nonlinear controller if the system is to behave according to design requirements. Non-smooth nonlinearities such as bi-linearity and freeplay are commonplace in joints and connections, but difficult to treat because of the abrupt changes in dynamic behaviour that occur as parts come into contact and separate. In this paper non-smooth nonlinearity is treated by the method of feedback linearisation [1–3], a nonlinear control method capable of transforming a nonlinear system into a linear one by appropriate choice of input. In complete input-output feedback linearisation all the states of a nonlinear system are linearised. This differs from the more general problem of partial input-output feedback linearisation, in which only the input-output map is linearised and the number of outputs is fewer than the number of states of the system. The remaining part of the system that has not been linearised generally remains nonlinear and is uncontrollable. Therefore its stability must be determined by checking the so-called zero dynamics; equivalent to a linear time invariant (LTI) system being minimum phase when all its zeros are in the left-hand half-plane. The method has found application in numerous engineering fields including

* Corresponding author.
E-mail addresses: domenico.lisitano@polito.it (D. Lisitano), S.Jiffri@liverpool.ac.uk (S. Jiffri), elvio.bonisoli@polito.it (E. Bonisoli), J.E.Mottershead@liverpool.ac.uk (J.E. Mottershead).

https://doi.org/10.1016/j.jsv.2017.11.047

Nomenclature

$\mathbf{A}$	State-space matrix for the zero dynamics
$\mathbf{b}$	Input vector
$\mathbf{C}$	Viscous damping matrix
$\mathbf{C_{nl}}$	Nonlinear damping matrix
f	objective function for linear model optimisation
$\mathbf{f_{Cnl}}$	Nonlinear damping force
$\mathbf{f_{Knl}}$	Nonlinear stiffness force
f_{n}	Desired natural frequency
$\mathbf{f}(t)$	Excitation force
g_1, g_2	left and right gaps: nonlinear spring
$g_{\mathrm{c,i}}$	Parameter correction factor
$\mathbf{g}_{\mathrm{q}}$	Force distribution vector
$\mathbf{K}$	Stiffness matrix
$\mathbf{K_{nl}}$	Nonlinear stiffness matrix
$k_{g,i}$	Stiffness of the spring between ith degree of freedom and the floor
k_{ij}	Stiffness of the spring between ith degree of freedom and jth degree of freedom
$k_{\mathrm{g,nl}}$	Nonlinear stiffness
$\mathbf{H}$	Receptance matrix
l_2	Vertical position of the nonlinear spring slider
$\mathbf{M}$	Mass matrix
m_i	Mass of the ith degree of freedom
n	Relative degree
$\mathbf{q}$	Displacement vector
$\mathbf{T}$	Transformation matrix
$\mathbf{T_{pl}}$	Transformation matrix of the controllable linerised coordinates
t	Time
$u(t)$	Real input
ν	Virtual input
$\mathbf{x}$	State space vector
$\mathbf{z}$	Linearised coordinate
$\mathbf{z}_{\mathrm{eq}}$	Equilibrium point
$\mathbf{z}_{\mathrm{id}}$	Internal dynamics
$\mathbf{z}_{\mathrm{zd}}$	Zero dynamics
$\dot{\bullet}$	First derivative with respect to time
$\ddot{\bullet}$	Second derivative with respect to time
$(\tilde{\bullet})$	Parameter nominal value
α	Viscous damping coefficient for mass proportionality
β	Viscous damping coefficient for stiffness proportionality
ε	Nonlinear damping force coefficient
η	Degree of freedom location of the nonlinearity
$\Omega(t)$	Time variant frequency for sweep excitation
ω_{n}	Desired natural frequency
χ	Output degree of freedom
ζ_{n}	Desired damping ratio

the following: robotics, to control the trajectory and the body posture of a mobile robot [4–7]; electric motors, to stabilise the position and velocity of the rotor and to control the voltage [8–12]; in fuel cells, to control the pressure of hydrogen and oxygen [13]; and in actuation systems with valve nonlinearities [14,15]. In aerospace engineering the technique is used to control drones [16,17] and to suppress wing flutter [18–20]. All these examples relate to smooth nonlinearities in the system or in the input, which means that there are no non-differentiable points in the nonlinear characteristic. The application of the feedback linearisation control to non-smooth nonlinear systems is an area open to research, possibly because the smoothness of the nonlinearity was originally said to be a requirement for the application of feedback linearisation. Tao and Kokotovic [21] proved this constraint to be unnecessary at least in cases where the non-smooth nonlinearity is in the input and has a dead zone, piecewise, backlash or hysteresis characteristic - for these cases they also developed adaptive methods. Jiffri et al. [22] developed the theory of complete and partial feedback linearisation to nonlinear aeroelastic systems with structural non-

smooth nonlinearity and demonstrated how flutter control of a wing might be achieved using a simulated example. In Ref. [23] this theory was applied experimentally to a non-smooth nonlinear system with the nonlinearity at the same degree of freedom as the input, thereby causing the zero dynamics of the system to be linear (i.e. a special case of partial feedback linearisation in which the entire system is linearised).

This paper is motivated by the need to generalise the experimental validation of feedback linearisation to non-smooth nonlinear systems, beyond the special case of [23], to include the more complicated general case when the zero dynamics are nonlinear. Partial feedback linearisation is applied to a non-smooth, nonlinear three degrees of freedom mass-spring system. In the present work the structural non-smooth stiffness and damping nonlinearity are located at a different degree of freedom from the output. The test-rig used in this study is presented in §2 with a full description of the system and its main characteristics. In §3, an analytical/numerical model is developed, and in §4 and §5 experimental tests on the linear and nonlinear configuration of the system, aimed at tuning the model parameters and validating it, are presented. In §s 6–8, feedback linearisation is applied theoretically to the system and the stability of the internal dynamics is checked. The control objective is to partially linearise the system while the remaining nonlinear part is made stable. Finally in §9 partial linearisation is demonstrated by assigning natural frequencies and damping ratios to the linearised subsystem, which in this case happens to be the motion of the first mass of the three degrees of freedom system. Both experimental and numerical results are presented, including the stable zero dynamics.

2. Experimental set-up

The experimental rig shown in Fig. 1 consists of three masses supported and connected by a set of thin plate-like springs. For simplicity the system degrees of freedom are numbered 1, 2 and 3 from left to right in the figure. The system is a very simple mechanical system, with a non-smooth piecewise spring located at the third degree of freedom.

The system overall dimensions are 38 × 33 cm. The non-smooth piecewise nonlinearity is achieved by means of two additional springs, which we will call setting springs, mounted either side of the third mass. Each setting spring is separated from a grounding (or support) spring by a continuously adjustable gap, g_1 on the left and g_2 on the right. The result is a non-smooth nonlinear hardening spring characteristic due to the different values of stiffness, shown in Fig. 2, when the gaps are open or closed. The nonlinear effect can be modified by changing the length of the setting spring l_2 (i.e. vertical contact location). The stiffness of the coupling (or connecting) springs can be also adjusted by changing the position of the upper rigid link. The settings chosen for the experiments carried out in this paper were $g_1 = g_2 = 0.035$ mm and $l_2 = 81.6$ mm.

Linearisation control was implemented in dSPACE using a nested controller with a model-based outer loop that provides an actuator command, applied in an inner PD control loop that sets the measured force applied at the first degree of freedom. Three laser displacement sensors (Keyence LK-500 and LK-G402 and microepsilon OptoNCDT 1402-100) were arranged to measure the horizontal displacements of the three masses and provide the dSPACE inputs. Control actuation was achieved using a LDS V406 permanent magnet shaker with a LDS PA100 amplifier. The shaker force was measured by a PCB 208C02 load cell with a PCB 442C04 ICP signal conditioner. Details of the experimental set-up can be seen in Fig. 3(a)–(c). The first subfigure shows the arrangement of masses and springs with the shaker attached at the first mass. The second subfigure is a close-up photograph of the non-smooth nonlinearity located at the third mass, and the complete arrangement can be seen in the third subfigure.

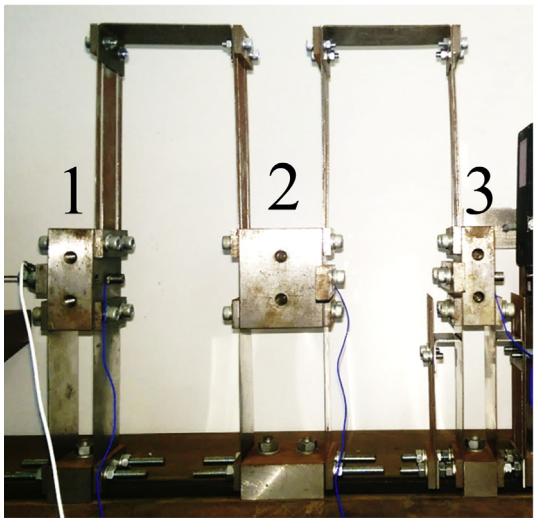

Fig. 1. Experimental test-rig.

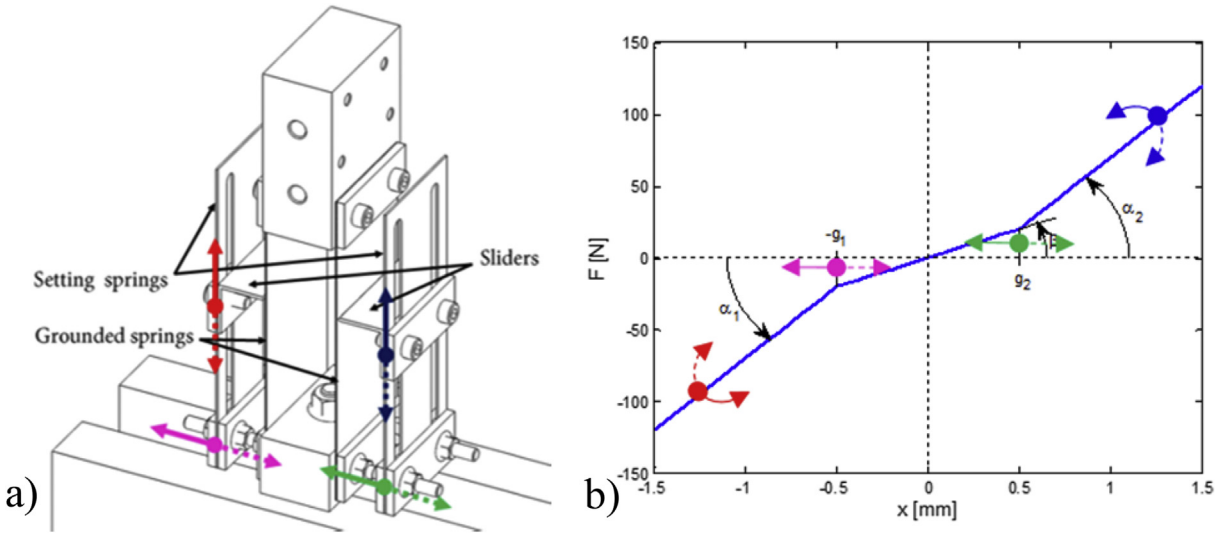

Fig. 2. a) Nonlinear spring model, b) Nonlinear spring characteristic.

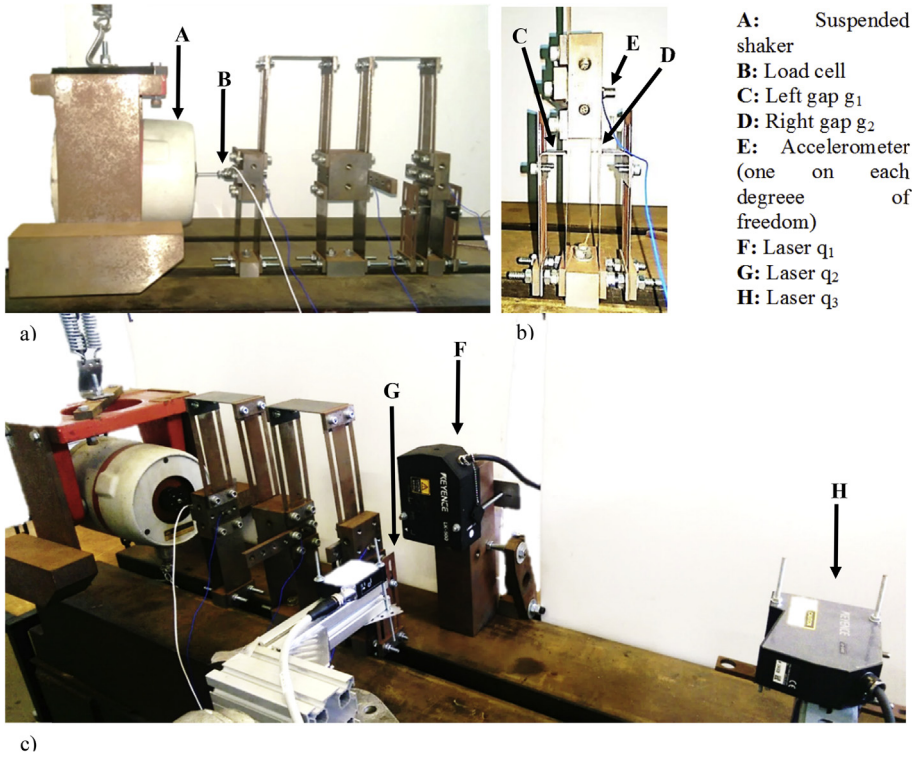

Fig. 3. (a)–(c) Details of the non-smooth nonlinear system experimental set-up.

The system was instrumented separately for (1) open-loop modal hammer testing of the linear system (setting springs removed), (2) stepped sine testing of the open-loop nonlinear system and (3) closed-loop modal hammer testing of the linearised system (with setting springs). The first two of these tests were required to tune the numerical model used in the third test. The tests were carried out using a LMS SCADAS III, an instrumented hammer PCB 086C03 and three Kistler accelerometers K-Shear 8728A500.

During closed-loop control the external input was provided by hammer excitation and modal properties of the linearised system were determined. The shaker was used to produce the linearising control input in real time. Displacements and

velocities, by differentiation, were measured using the laser sensors. Both displacement and force signals were filtered using a second-order Butterworth filter with a cut-off frequency of 21 Hz, to remove high frequency noise and disturbances but without removing frequencies components related to the natural frequencies of the system or to the desired natural frequency of the linearised portion (maximum 19 Hz).

3. System model

The test rig may be represented schematically as the three degrees of freedom lumped parameter system shown in Fig. 4. The masses are assumed to be rigid and the springs massless. The nonlinear spring is located at the third mass.

In theory the nonlinear spring introduces piecewise nonlinear behaviour in the stiffness, but in practice nonlinear damping is also present, due to the effects of friction and impact. The equation of motion may be written in the time domain as,

$$\mathbf{M}\ddot{\mathbf{q}} + \mathbf{C}\dot{\mathbf{q}} + \mathbf{K}\,\mathbf{q} + \mathbf{f}_{\mathbf{Knl}} + \mathbf{f}_{\mathbf{Cnl}} = \mathbf{f}(t) \tag{1}$$

where $\mathbf{q}$ contains the displacements associated with the three degrees of freedom, $\mathbf{M}$, $\mathbf{C}$ and $\mathbf{K}$ are the mass, damping and stiffness matrices respectively, $\mathbf{f}_{\mathbf{Knl}}$ is the vector of nonlinear forces due to the nonlinear stiffness, $\mathbf{f}_{\mathbf{Cnl}}$ is the vector of nonlinear forces due to nonlinear damping and $\mathbf{f}(t)$ is the excitation applied to the system. The structure and parameters pertaining to the above quantities may be expressed in the form,

$$\mathbf{q} = \{\, q_1 \quad q_2 \quad q_3 \,\}^{\mathrm{T}} \Rightarrow \dot{\mathbf{q}} = \{\, \dot{q}_1 \quad \dot{q}_2 \quad \dot{q}_3 \,\}^{\mathrm{T}} \Rightarrow \ddot{\mathbf{q}} = \{\, \ddot{q}_1 \ddot{q}_2 \ddot{q}_3 \,\}^{\mathrm{T}}; \mathbf{M} = \mathrm{diag}(m_1, m_2, m_3)$$

$$\mathbf{K} = \begin{bmatrix} 2k_{g,1} + k_{12} & -k_{12} & 0 \\ -k_{12} & 2k_{g,2} + k_{12} + k_{23} & -k_{23} \\ 0 & -k_{23} & 2k_{g,3} + k_{23} \end{bmatrix}; \quad \mathbf{C} = \alpha\ \mathbf{M} + \beta\ \mathbf{K}; \quad \mathbf{f}(t) = \begin{Bmatrix} 1 \\ 0 \\ 0 \end{Bmatrix} u(t) \tag{2}$$

The complete definition of the nonlinear spring stiffness is shown in Fig. 2 and may be written formally as,

$$k_{g,\mathrm{nl}} = \begin{cases} 2k_{g,3} + k_2 & q_3 \le -g_1 \\ 2k_{g,3} & -g_1 \le q_3 \le g_2 \\ 2k_{g,3} + k_2 & q_3 \ge g_2 \end{cases} \tag{3}$$

and the nonlinear stiffness force in Eq. (2) is then given by,

$$\mathbf{f}_{\mathbf{Knl}} = \begin{cases} \mathbf{K}_{\mathbf{nl}}\left(\mathbf{q} - \{0, 0, -g_1\}^{\mathrm{T}}\right) & \text{if } q_3 < -g_1 \\ \mathbf{0} & \text{if } -g_1 \le q_3 \le g_2; \\ \mathbf{K}_{\mathbf{nl}}\left(\mathbf{q} - \{0, 0, g_2\}^{\mathrm{T}}\right) & \text{if } q_3 > g_2 \end{cases} \quad \mathbf{K}_{\mathbf{nl}} = \begin{bmatrix} 0 & 0 & 0 \\ 0 & 0 & 0 \\ 0 & 0 & k_2 \end{bmatrix} \tag{4}$$

Energy is dissipated mainly as Coulomb friction between the slider and the grounding spring, so that the damping is proportional to the nonlinear stiffness force. The nonlinear damping force is modelled equivalently by taking into

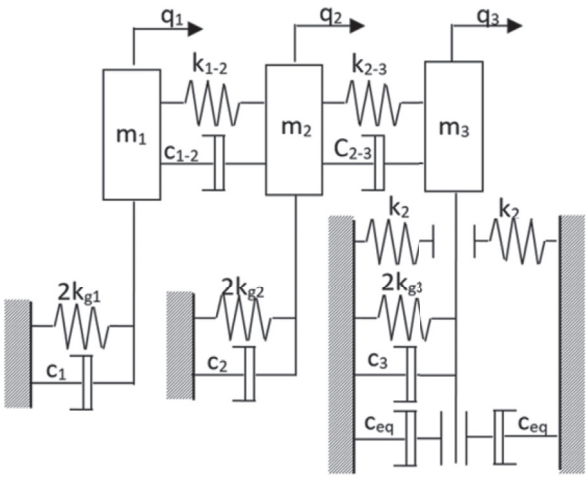

Fig. 4. Schematic of the three degrees of freedom non-smooth nonlinear system.

consideration the physical assumption just described; it acts only when the slider and the setting spring are in contact and may be written as:

$$f_{\mathrm{Cnl},3} = \varepsilon |f_{\mathrm{Knl},3}| \mathrm{sgn}(\dot{q}_3) \tag{5}$$

where ε is a correction factor to take account of friction and the impact restitution factor, while $|f_{\mathrm{Knl},3}|$ is the contact force. The nonlinear damping force can then be expressed as,

$$\mathbf{f_{Cnl}} = \mathbf{C_{nl}} |\mathbf{f_{Knl}}| \mathrm{sgn}(\dot{q}_3); \quad \mathbf{C_{nl}} = \begin{bmatrix} 0 & 0 & 0 \\ 0 & 0 & 0 \\ 0 & 0 & \varepsilon \end{bmatrix} \tag{6}$$

Tuning of the system parameters was found to be necessary to converge the model upon the linear and nonlinear dynamics of the system.

4. Tuning the linear parameters

The set of linear parameters consists of the three masses of the system, the stiffness of the coupling and grounding springs and the proportional coefficients of the viscous damping model. An experimental hammer test was carried out on the linear system, with the setting springs removed, to determine the complete experimental receptance matrix with a frequency resolution of 0.05 Hz and averaging over 5 excitations with the hammer. Natural frequencies, damping ratios and mode shapes were extracted using the Polymax algorithm [24]. An optimisation procedure using an Immune Network Model Optimisation method [25] was used to minimise the difference between the experimental frequency response functions (FRFs) and those produced by the tuned numerical model in the range between 5 and 15 Hz. Ten independent parameters (3 masses, 5 stiffness and 2 proportional viscous coefficients) were optimised using the objective function,

$$f = \sum_{i=1}^{3} \sum_{j=1}^{3} \sum_{k} \left(FRF_{i,j\ \mathrm{num}} - FRF_{i,j\ \mathrm{exp}} \right)^2 \tag{7}$$

where i and j denote the degree of freedom of the system and k is the spectral-line index. The optimised parameters are shown in Table 1, where $(\tilde{\bullet})$ denotes a nominal value and $(\bullet)_i = g_{c,i}(\tilde{\bullet})_i$ is a tuned (optimised) parameter. The correction factors, $g_{c,i}$, close to unity, are deemed to be physical; the springs are found to be slightly softer than the numerical stiffnesses and the masses of the springs, neglected in the analysis, are spread across the three lumped masses of the system.

The FRFs, shown in Fig. 5, confirm that the system is indeed linear and the tuned model is in very good agreement with experimental results, showing only small discrepancies at very low levels of response. Fig. 6 shows that natural frequencies determined from the tuned model are very close to measured values and mode shapes are in excellent agreement (MAC > 99.5%).

5. Tuning the nonlinear parameters

The nonlinear stiffness and damping parameters, k_2 and ε, were tuned using data from stepped sine tests carried out forwards and backwards in the range 5 Hz–35 Hz in steps of 0.05 Hz. Constant-amplitude force excitation was delivered by a suspended and balanced shaker, with different constant amplitudes for each of four experiments performed. The results obtained from each experiment were averaged over three tests at the same level of force amplitude.

The effect of the hardening nonlinearity is most clearly evident in the FRFs $\mathbf{H}_{1,3}$ shown in Fig. 7. The excitation force was controlled to remain within ±0.05 N of the desired value. When the force increases the peak of the third mode becomes

Table 1
Linear system parameters.

Parameter		Correction factor	
$\tilde{k}_{g,1}$	1808.7 N/m	$g_{c,1}$	0.870027004224418
$\tilde{k}_{g,2}$	1808.7 N/m	$g_{c,2}$	0.876885639694682
$\tilde{k}_{g,3}$	1808.7 N/m	$g_{c,3}$	1.107066723916180
$\tilde{k}_{12}$	1735.5 N/m	$g_{c,4}$	0.603583985626064
$\tilde{k}_{23}$	1735.5 N/m	$g_{c,5}$	0.726010104919688
$\tilde{m}_1$	1.3297 kg	$g_{c,6}$	0.890575720110895
$\tilde{m}_2$	2.4234 kg	$g_{c,7}$	0.955704101276241
$\tilde{m}_3$	0.9065 kg	$g_{c,8}$	1.299946099547680
$\tilde{\alpha}$	0.2605	$g_{c,9}$	0.926541049902140
$\tilde{\beta}$	2.7948e-5	$g_{c,10}$	1.005752187189990

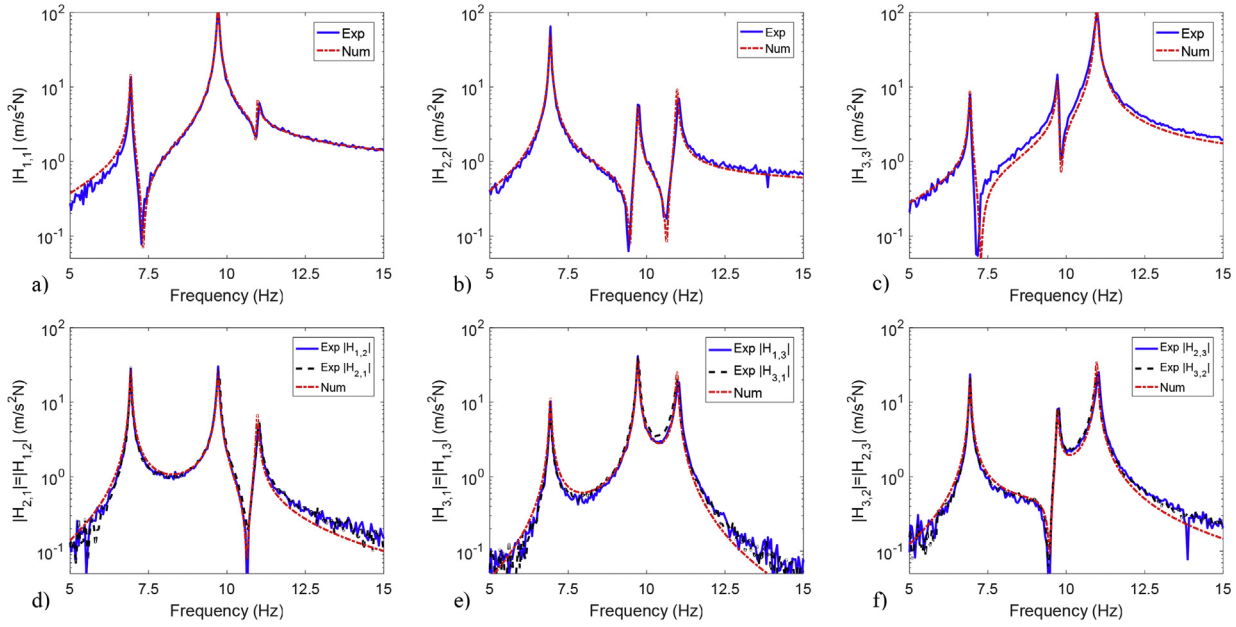

Fig. 5. (a)–(f) Experimental and numerical FRF comparison.

increasingly distorted, the resonant amplitude decreases and the jump frequency increases. Minor peaks at around 8 Hz, which do not appear in the linear test, are the effect of the shaker added mass linked to the system through the stinger [26].

Numerical nonlinear FRFs were obtained from the envelope of the time domain response of the system, excited at the first degree of freedom with a sine-sweep in which the excitation frequency $\Omega(t)$ varied linearly with time, but slowly compared to the natural periods of the system. The FRFs were found to be sensitive to the nonlinear parameters only in the frequency range of the third mode, most affected by the nonlinear degree of freedom. The jump frequency is mainly influenced by the coefficient ε and by increasing ε the jump was found to occur at lower frequencies as a result of increased damping. The setting-spring stiffness k_2 was found to affect the slope of the FRFs around the nonlinear mode and the onset of nonlinearity was determined according to the sizes of the gaps g_1 and g_2, measured using a feeler gauge. Manually tuned parameters $\varepsilon = 0.3954$, $k_2 = 1722.6$ N were found to produce numerical FRFs in very close agreement with measured values.

The comparison between experimental and numerical FRFs obtained with both upward and downward stepped-sines at four different levels of excitation is shown in Fig. 8. The FRF obtained for downward stepped-sine tests are very similar to those obtained during upward excitation; some differences are visible only in the jump frequencies, as is usual in nonlinear hardening systems. The comparison between experimental and numerical results confirms that the mathematical model is sufficiently accurate to describe the nonlinear behaviour of the system.

6. Feedback linearisation theory

The theory of feedback linearisation for systems with non-smooth nonlinearity was established by Jiffri et al. [22]. Feedback linearisation can be applied to linearise the complete system or only certain chosen degrees of freedom by replacing the nonlinear dynamics with arbitrarily-chosen linear dynamics. In the present case, input-output partial feedback linearisation is implemented by means of a virtual input and a coordinate transformation to linearise the nonlinear system often described as [1–3,18],

$$\dot{\mathbf{x}} = \mathbf{f}(\boldsymbol{x}) + \mathbf{g}(\boldsymbol{x})u(t); \quad u(t) = \varphi(\mathbf{x}) + \rho(\mathbf{x})\nu(t); \quad \mathbf{z} = \mathbf{T}\mathbf{x}; \quad \mathbf{x} = \{\,\mathbf{q} \quad \dot{\mathbf{q}}\,\}^{\mathrm{T}} \tag{8}$$

where $u(t)$ is the real input to the nonlinear system, $\nu(t)$ is a "virtual input" corresponding to the linearised system, $\mathbf{z}$ is the linearised state vector and $\mathbf{T}$ is the co-ordinate transformation matrix. The nonlinear system described in Eq. (1) may be cast in first order form as,

$$\dot{\mathbf{x}} = \mathbf{f}(\mathbf{x}) + \mathbf{g}(\mathbf{x})u(t) \tag{9}$$

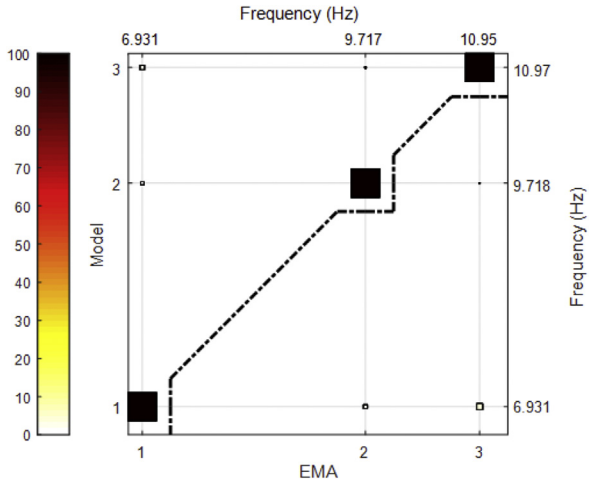

Fig. 6. MAC between numerical and experimental mode shapes.

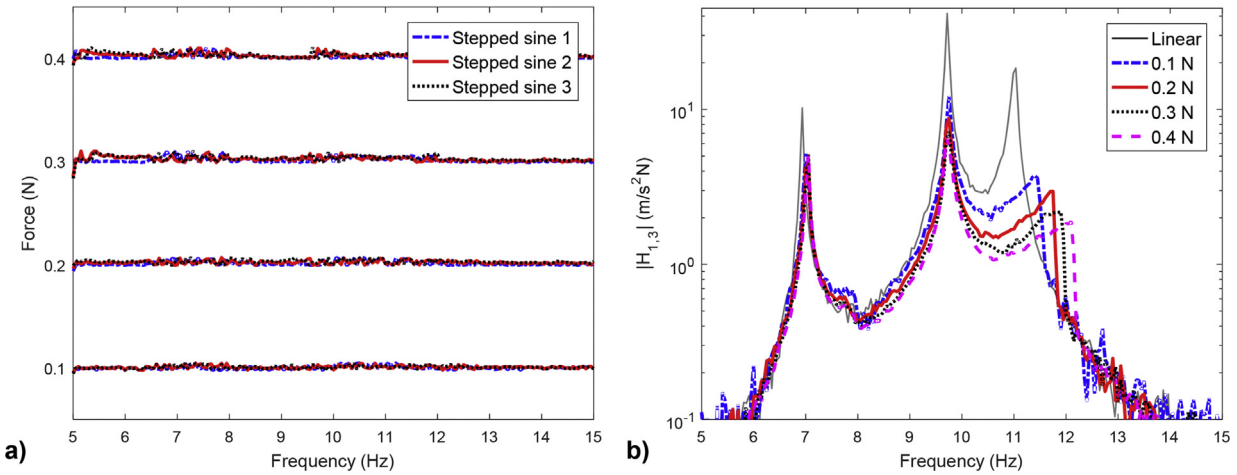

Fig. 7. Nonlinear experimental FRF for different levels of excitation - downward sweep: a) excitation force amplitude, b) nonlinear system responses.

$$\mathbf{f}(\mathbf{x}) = \begin{Bmatrix} \mathbf{x}_{(4:6)} \\ -\mathbf{M}^{-1}(\mathbf{K}\mathbf{x}_{(1:3)} + \mathbf{C}\mathbf{x}_{(4:6)} + \mathbf{f}_{\mathbf{knl}}(\mathbf{x}_{(1:3)}) + \mathbf{f}_{\mathbf{cnl}}(x_3, x_6)) \end{Bmatrix}$$
$$\mathbf{g}(\mathbf{x}) = \begin{Bmatrix} \mathbf{0}_{(3x1)} \\ \mathbf{M}^{-1}\mathbf{g}_q \end{Bmatrix}; \quad \mathbf{g}_q = \begin{pmatrix} 1 \\ 0 \\ 0 \end{pmatrix} \tag{10}$$

The displacement at the first degree of freedom, q_1, is chosen as the output y, for the input-output linearisation procedure, while the nonlinearity is located in the third degree of freedom. The complete set of equations representing the partially linearised system is obtained by combining the output equation with its n time-derivatives, where n is the relative degree of the single input single output (SISO) system, i.e. the number of times it is necessary to differentiate the output before the input term appears explicitly. Denoting the coordinates of the linearised system as $z_{i=1,2}$,

$$z_1 = y = x_1 \tag{11}$$

$$z_2 = \dot{z}_1 = \dot{y} = \dot{x}_1 = x_4 \tag{12}$$

$$\dot{z}_2 = \ddot{z}_1 = \ddot{y} = \dot{x}_1 = \dot{x}_4 = f_4(\mathbf{x}) + g_4(\mathbf{x})u(t) \tag{13}$$

where $f_4(\mathbf{x})$ and $g_4(\mathbf{x}) \neq 0$, are the 4^{th} rows of the vectors $\mathbf{f}(\mathbf{x})$ and $\mathbf{g}(\mathbf{x})$ respectively. Thus, the relative degree of the system is $n = 2$, from which it is evident that the linearisation of the system is partial because n is less than the dimension of the state

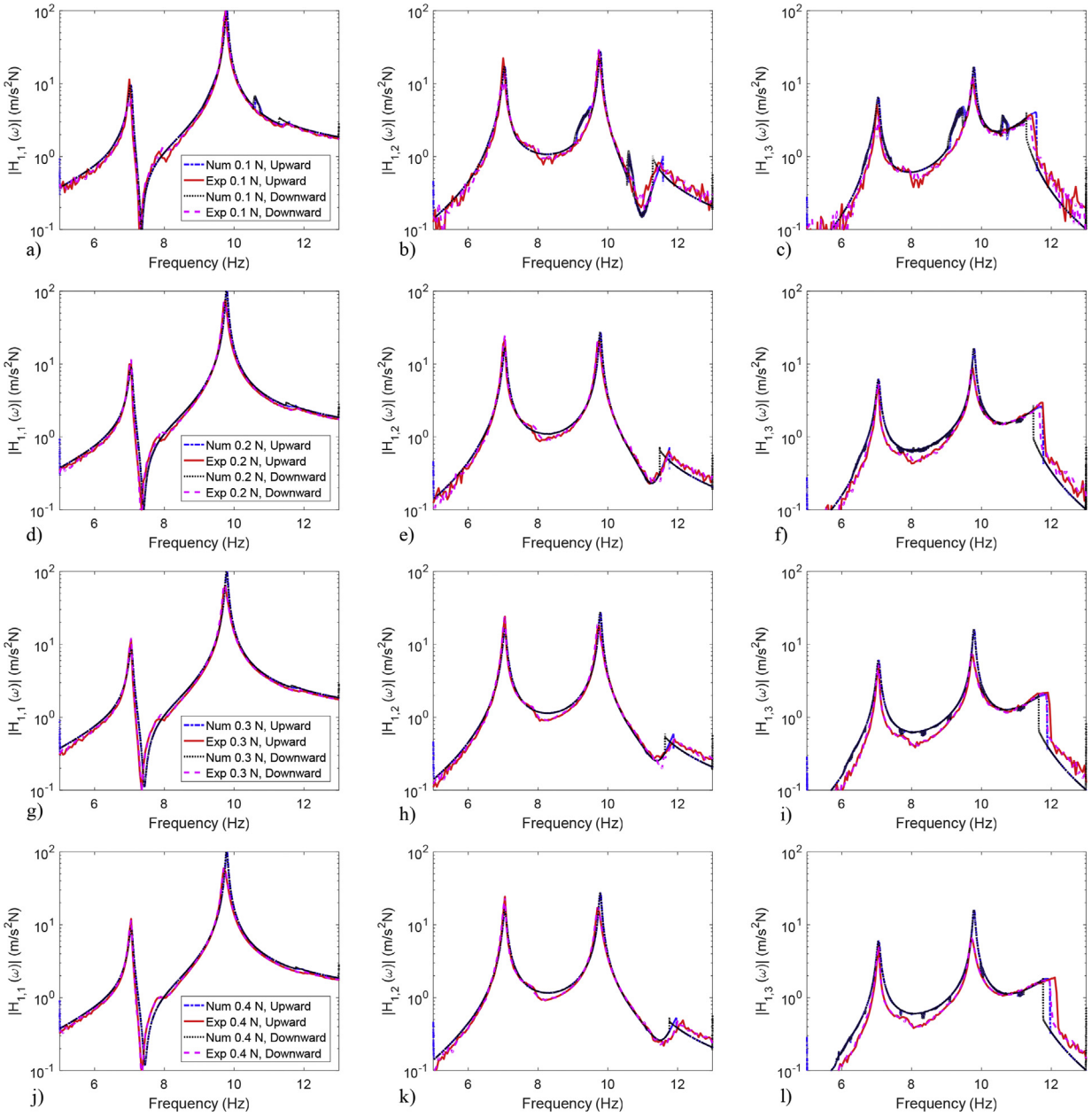

Fig. 8. Experimental vs. numerical FRFs, with changing force amplitude: (a)–(c) $F = 0.1$ N, (d)–(f) $F = 0.2$ N, (g)–(i) $F = 0.3$ N, (j)–(l) $F = 0.4$ N.

vector $\mathbf{x}$. It is shown in Appendix B that feedback linearisation is not feasible for lumped mass systems with the input and output at different degrees of freedom. Therefore, for the lumped mass non-smooth nonlinear system the input and output must be at the same degrees of freedom in order to apply feedback linearisation control. The transformation matrix between the linear and nonlinear systems of coordinates may be obtained from Eqs. (12) and (13) as,

$$\begin{Bmatrix} z_1 \\ z_2 \end{Bmatrix} = \mathbf{T_{pl}}\mathbf{x} = \begin{bmatrix} 1 & 0 & 0 & 0 & 0 & 0 \\ 0 & 0 & 0 & 1 & 0 & 0 \end{bmatrix} \{\mathbf{x}\} \tag{14}$$

The system in linear coordinates becomes,

$$\begin{Bmatrix} \dot{z}_1 \\ \dot{z}_2 \end{Bmatrix} = \begin{bmatrix} 0 & 1 \\ 0 & 0 \end{bmatrix} \begin{Bmatrix} z_1 \\ z_2 \end{Bmatrix} + \begin{Bmatrix} 0 \\ 1 \end{Bmatrix} v, \quad v = f_4(\mathbf{x}) + g_4(\mathbf{x})u(t) \tag{15}$$

where ν is the artificial input, which may be chosen to specify the dynamics of the linearised system by eigenvalue assignment,

$$v = -r_1 z_1 - r_2 z_2 = -\omega_n^2 z_1 - 2\zeta_n \omega_n z_2 \tag{16}$$

It is found by substituting Eq. (16) into Eq. (15) that,

$$\begin{Bmatrix} \dot{z}_1 \\ \dot{z}_2 \end{Bmatrix} = \begin{bmatrix} 0 & 1 \\ -\omega_n^2 & -2\zeta_n \omega_n \end{bmatrix} \begin{Bmatrix} z_1 \\ z_2 \end{Bmatrix} \tag{17}$$

7. Internal dynamics

It is generally not possible to control the entire dynamics of a multi degree of freedom system using a single output. In the present case the system described in Eq. (17) has a dimension of 2 whereas the full system has dimension 6. Thus, there remains an un-linearised portion of dimension 4, known as the internal dynamics. The full transformation matrix **T**, where $\mathbf{z} = \mathbf{T}\,\mathbf{x}$, should be chosen under the conditions (a) that it is non-singular and (b) the dynamics associated with the additional co-ordinates are orthogonal to $\mathbf{g}(\mathbf{x})$. The latter condition ensures that the internal dynamics are obtained in the normal form, where the system inputs do not appear. A matrix satisfying these conditions is given by,

$$\mathbf{z} = \mathbf{T}\mathbf{x}, \quad \mathbf{T} = \begin{bmatrix} 1 & 0 & 0 & 0 & 0 & 0 \\ 0 & 0 & 0 & 1 & 0 & 0 \\ 0 & 1 & 0 & 0 & 0 & 0 \\ 0 & 0 & 1 & 0 & 0 & 0 \\ 0 & 0 & 0 & 0 & 1 & 0 \\ 0 & 0 & 0 & 0 & 0 & 1 \end{bmatrix} \tag{18}$$

and the nonlinear internal dynamics in transformed coordinates may then be written as,

$$\dot{\mathbf{z}}_{id} = \begin{Bmatrix} \dot{z}_3 \\ \dot{z}_4 \\ \dot{z}_5 \\ \dot{z}_6 \end{Bmatrix} = \begin{bmatrix} 0 & 0 & 0 & 0 & 1 & 0 \\ 0 & 0 & 0 & 0 & 0 & 1 \\ \frac{k_{1,2}}{m_2} & -\frac{c_{2,1}}{m_2} & -\frac{2k_{g,2}+k_{1,2}+k_{2,3}}{m_2} & \frac{k_{2,3}}{m_2} & -\frac{c_{2,2}}{m_2} & -\frac{c_{2,3}}{m_2} \\ 0 & -\frac{c_{3,1}}{m_3} & \frac{k_{2,3}}{m_3} & -\frac{k_{2,3}+2k_{g,3}}{m_3} & -\frac{c_{3,2}}{m_3} & -\frac{c_{3,3}}{m_3} \end{bmatrix} \begin{Bmatrix} z_1 \\ z_2 \\ z_3 \\ z_4 \\ z_5 \\ z_6 \end{Bmatrix} + \\ + [0 \quad 0 \quad 0 \quad -1/m_3]^{\mathrm{T}} \left(f_{\mathrm{Knl}_3}(z_4) + f_{\mathrm{Cnl}_3}(z_4, \dot{z}_4)\right) \tag{19}$$

where $c_{i,j}$ is the element located at i^{th} row and j^{th} column of the damping matrix **C**. The so-called zero dynamics are found by setting to zero the coordinates z_1 and z_2 corresponding to the linearised state variables. Thus,

$$\dot{\mathbf{z}}_{zd} = \begin{Bmatrix} \dot{z}_3 \\ \dot{z}_4 \\ \dot{z}_5 \\ \dot{z}_6 \end{Bmatrix} = \begin{bmatrix} 0 & 0 & 1 & 0 \\ 0 & 0 & 0 & 1 \\ -\frac{2k_{g,2}+k_{1,2}+k_{2,3}}{m_2} & \frac{k_{2,3}}{m_2} & -\frac{c_{2,2}}{m_2} & -\frac{c_{2,3}}{m_2} \\ \frac{k_{2,3}}{m_3} & -\frac{k_{2,3}+2k_{g,3}}{m_3} & -\frac{c_{3,2}}{m_3} & -\frac{c_{3,3}}{m_3} \end{bmatrix} \begin{Bmatrix} z_3 \\ z_4 \\ z_5 \\ z_6 \end{Bmatrix} + \\ + [0 \quad 0 \quad 0 \quad -1/m_3]^{\mathrm{T}} \left(f_{\mathrm{Knl}_3}(z_4) + f_{\mathrm{Cnl}_3}(z_4, \dot{z}_4)\right) \tag{20}$$

Then, with the proviso that the dynamics of the linearised system are stable by eigenvalue assignment, stability of the complete system is ensured when the zero dynamics are stable. Proof of the stability of the zero dynamics may be found in Appendix A and demonstrated in numerical simulations with different initial conditions in Fig. 9.

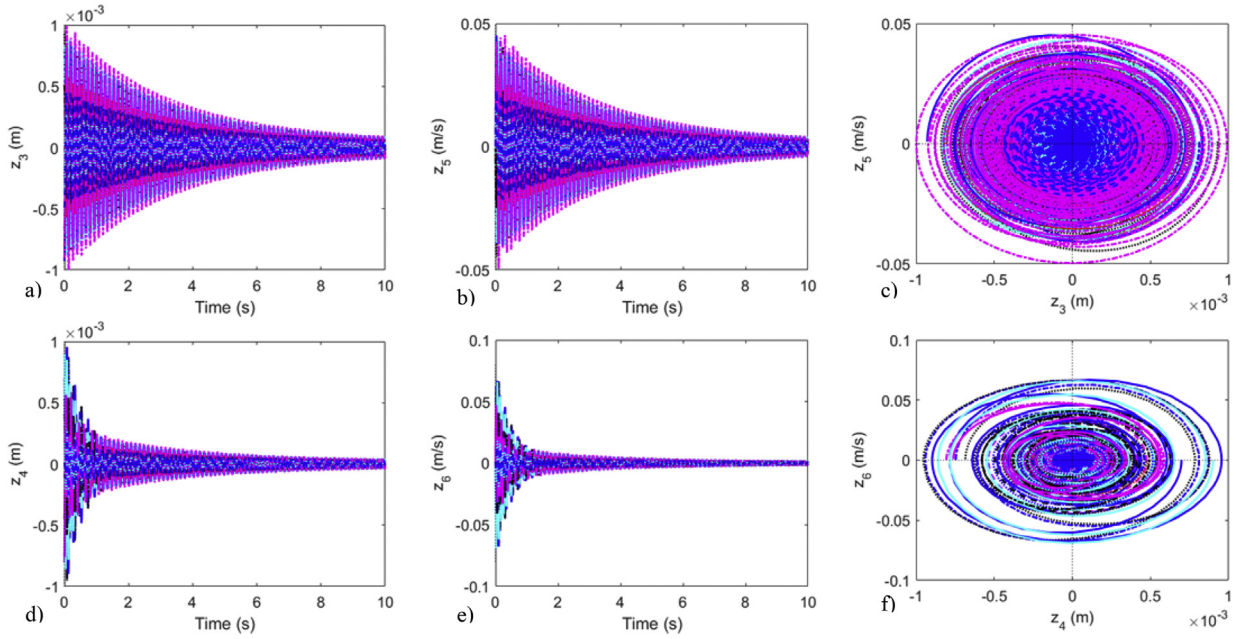

Fig. 9. Several numerical simulations of the internal dynamics with different initial conditions: (a),(b),(d),(e) time-domain responses and (c),(f) phase portraits.

8. Dynamics of the complete system with partial feedback linearisation

The equation describing the complete dynamics of the partially linearised system can be expressed using Eqs. (17) and (19) as,

$$\dot{\mathbf{z}} = \begin{Bmatrix} \dot{z}_1 \\ \dot{z}_2 \\ \dot{z}_3 \\ \dot{z}_4 \\ \dot{z}_5 \\ \dot{z}_6 \end{Bmatrix} = \begin{bmatrix} 0 & 1 & 0 & 0 & 0 & 0 \\ -\omega_n^2 & -2\zeta_n\omega_n & 0 & 0 & 0 & 0 \\ 0 & 0 & 0 & 0 & 1 & 0 \\ 0 & 0 & 0 & 0 & 0 & 1 \\ \dfrac{k_{1,2}}{m_2} & -\dfrac{c_{2,1}}{m_2} & -\dfrac{2k_{g,2}+k_{1,2}+k_{2,3}}{m_2} & \dfrac{k_{2,3}}{m_2} & -\dfrac{c_{2,2}}{m_2} & -\dfrac{c_{2,3}}{m_2} \\ 0 & -\dfrac{c_{3,1}}{m_3} & \dfrac{k_{2,3}}{m_3} & -\dfrac{k_{2,3}+2k_{g,3}}{m_3} & -\dfrac{c_{3,2}}{m_3} & -\dfrac{c_{3,3}}{m_3} \end{bmatrix} \begin{Bmatrix} z_1 \\ z_2 \\ z_3 \\ z_4 \\ z_5 \\ z_6 \end{Bmatrix} + \\ + [0 \quad 0 \quad 0 \quad 0 \quad 0 \quad -1/m_3]^{\mathrm{T}} (f_{\mathrm{Knl}_3}(z_4) + f_{\mathrm{Cnl}_3}(z_4, \dot{z}_4)) \tag{21}$$

It is seen that the linearised part is given entirely in terms of the first two states and is therefore independent of states $z_3 - z_6$. The nonlinear internal dynamics depend upon the full system of states including z_1, z_2 of the linearised sub-system. This effect is also apparent when the system in Eq. (21) is re-written in second order form,

$$\begin{bmatrix} 1 & 0 & 0 \\ 0 & m_2 & 0 \\ 0 & 0 & m_3 \end{bmatrix} \begin{Bmatrix} \ddot{z}_1 \\ \ddot{z}_3 \\ \ddot{z}_4 \end{Bmatrix} + \begin{bmatrix} 2\zeta_n\omega_n & 0 & 0 \\ -\beta k_{12} & \alpha m_2 + \beta(k_{g,2} + k_{12} + k_{23}) & -\beta k_{23} \\ 0 & -\beta k_{23} & \alpha m_3 + \beta(k_{g,3} + k_{23}) \end{bmatrix} \begin{Bmatrix} \dot{z}_1 \\ \dot{z}_3 \\ \dot{z}_4 \end{Bmatrix} + \\ + \begin{bmatrix} \omega_n^2 & 0 & 0 \\ -k_{12} & k_{g,2} + k_{12} + k_{23} & -k_{23} \\ 0 & -k_{23} & k_{g,3} + k_{23} \end{bmatrix} \begin{Bmatrix} z_1 \\ z_3 \\ z_4 \end{Bmatrix} + \begin{Bmatrix} 0 \\ 0 \\ f_{\mathrm{Knl}_3} \end{Bmatrix} + \begin{Bmatrix} 0 \\ 0 \\ f_{\mathrm{Cnl}_3} \end{Bmatrix} = \begin{Bmatrix} 0 \\ 0 \\ 0 \end{Bmatrix} \tag{22}$$

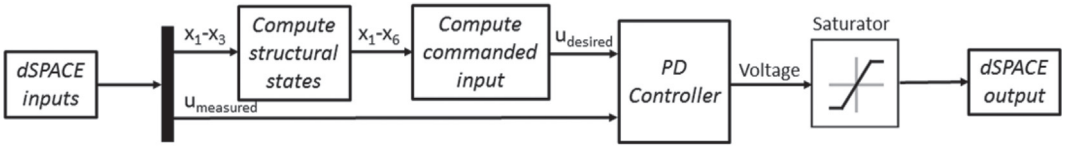

Fig. 10. Schematic of the control strategy.

The system damping and stiffness matrices have lost the property of symmetry, the eigenvalue of the linear first degree of freedom is the assigned natural frequency $\omega_n = 2\pi f_n$ with damping ratio ζ_n, and the system corresponding to the second and third degrees of freedom is nonlinear.

9. Results

In this section experimental and numerical results from the three degrees of freedom, non-smooth, nonlinear, closed-loop system are presented and compared.

The experimental setup was the described in §2 including the use of dSPACE for implementation of the controller and LMS Test.Lab for external hammer excitation of the linearised system. The first degree of freedom should be linear when the controller is switched on and therefore an impact modal test is entirely appropriate. The closed-loop test procedure begins with the system in static equilibrium. Desired ω_n and ζ_n are set and the controller is switched on. Hammer excitation is delivered at the first mass and displacement and accelerations are measured at all three masses. The shaker delivers the

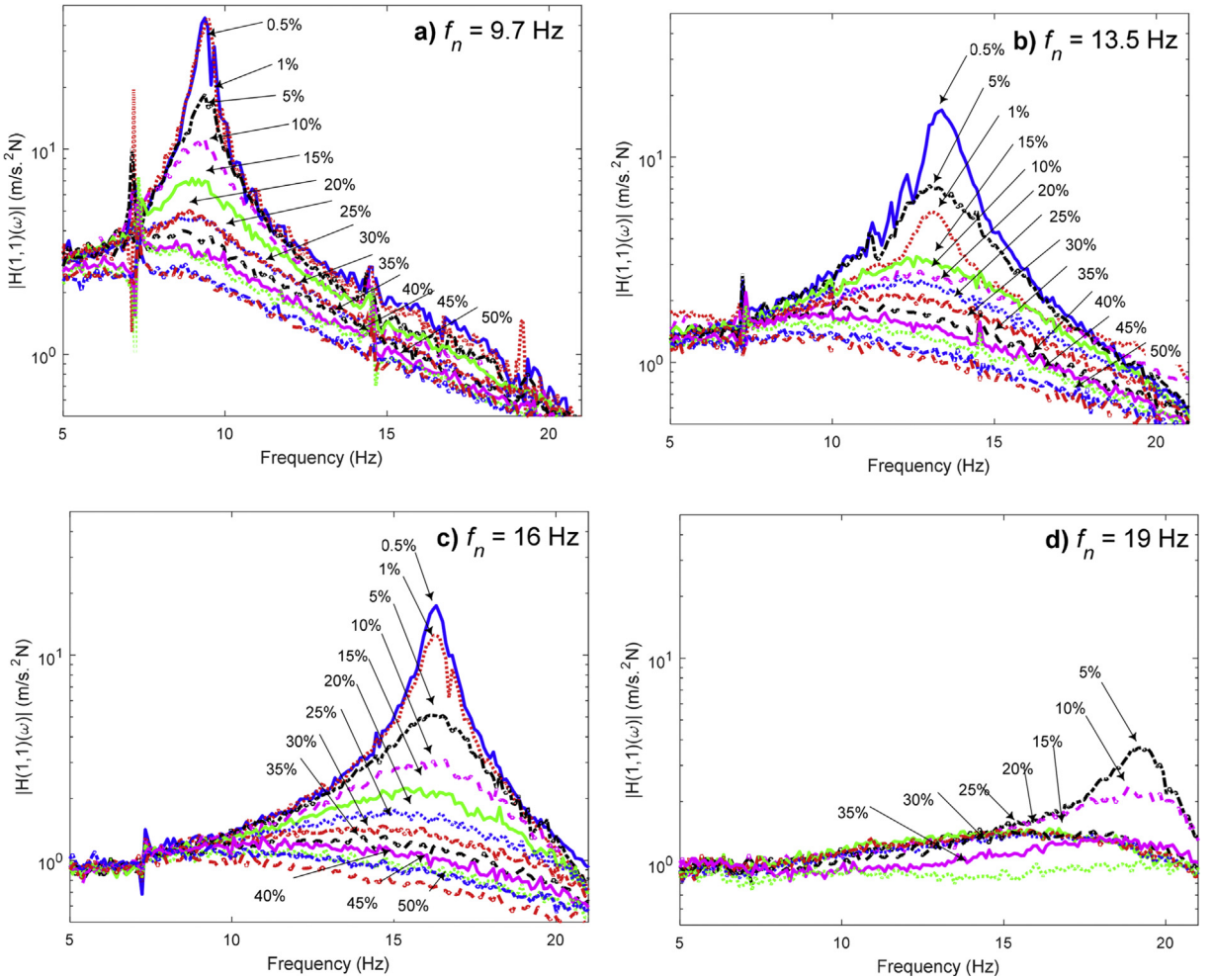

Fig. 11. (a–d) Experimental closed-loop FRFs.

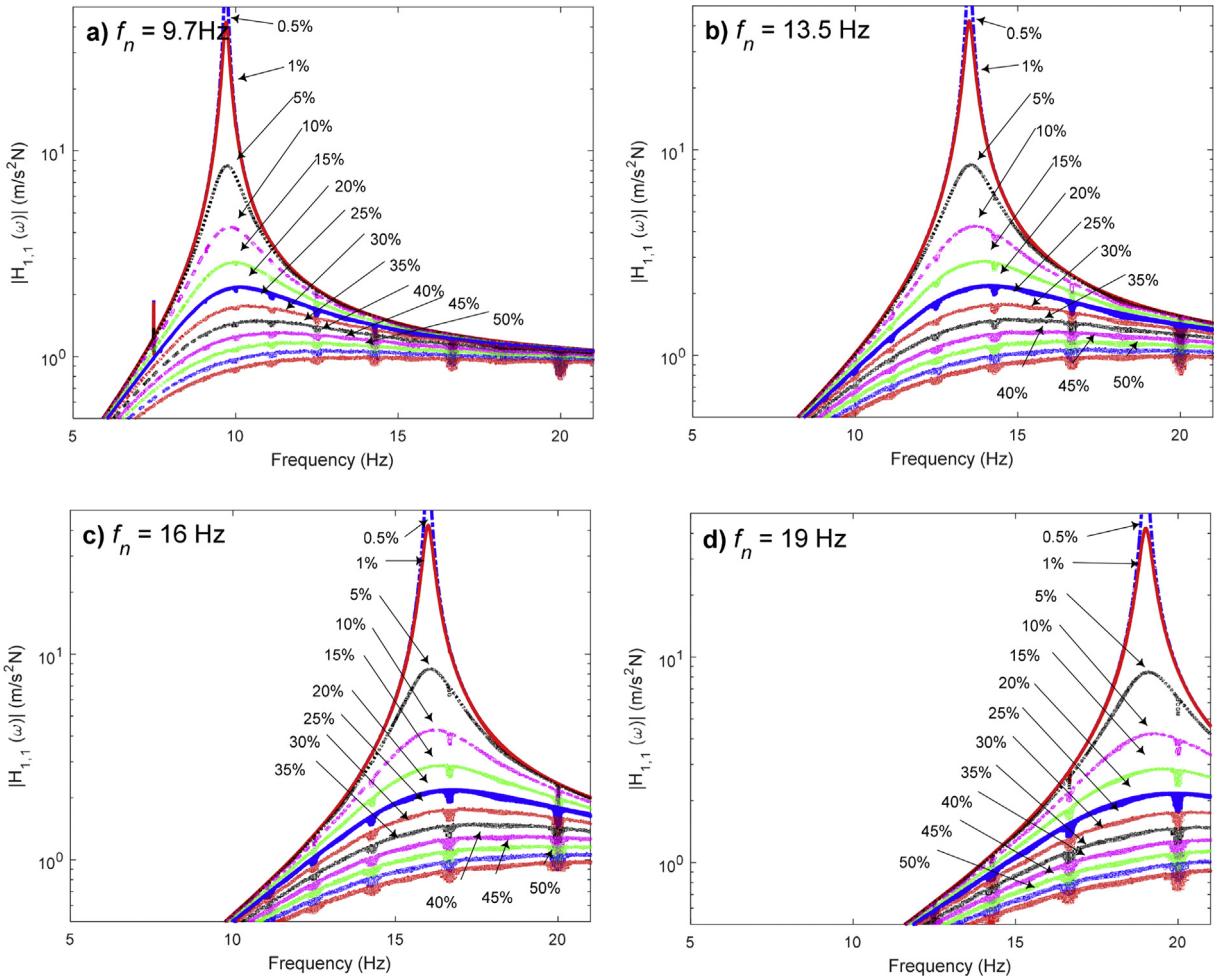

Fig. 12. (a–d) Numerical closed-loop FRFs.

control force according to the commanded input determined by the dSPACE model (at 10 kHz processing speed) and regulated by the PD controller. The duration of a single test from the moment of impact is 10 s, experimental FRFs are obtained in LMS Test.Lab by averaging over 5 tests and modal parameters of the linearised system are determined.

A schematic of the closed-loop control is shown in Fig. 10 with the outer dSPACE control loop and the inner PD controller, which was tuned separately on a sinusoidal signal with gains that were feasible for the working frequency range of the system – further details can be found in Appendix C. The purpose of the saturation term is to prevent damage to the shaker caused by hitting the stops at the end of its stroke.

Numerical closed-loop FRFs were obtained for purposes of comparison by exciting the partially linearised model with a slowly varying sine-swept force applied at the first degree of freedom. The equation of motion includes both the external excitation $f(t) = \sin(\Omega(t)t)$ and the control force $u(t)$,

$$\mathbf{M}\ddot{\mathbf{q}} + \mathbf{C}\dot{\mathbf{q}} + \mathbf{K}\mathbf{q} + \mathbf{f}_{\mathbf{Knl}} + \mathbf{f}_{\mathbf{Cnl}} = \mathbf{g}_q(f(t) + u(t)) \tag{23}$$

where $\Omega(t)$ changes linearly with time at a slow rate compared to the natural frequencies of the system.

Experiments and numerical simulations were repeated for four different values of natural frequencies,

$$f_{\mathrm{n}} = \{9.7 \quad 13.5 \quad 16 \quad 19\}\mathrm{Hz}$$

and twelve damping ratios,

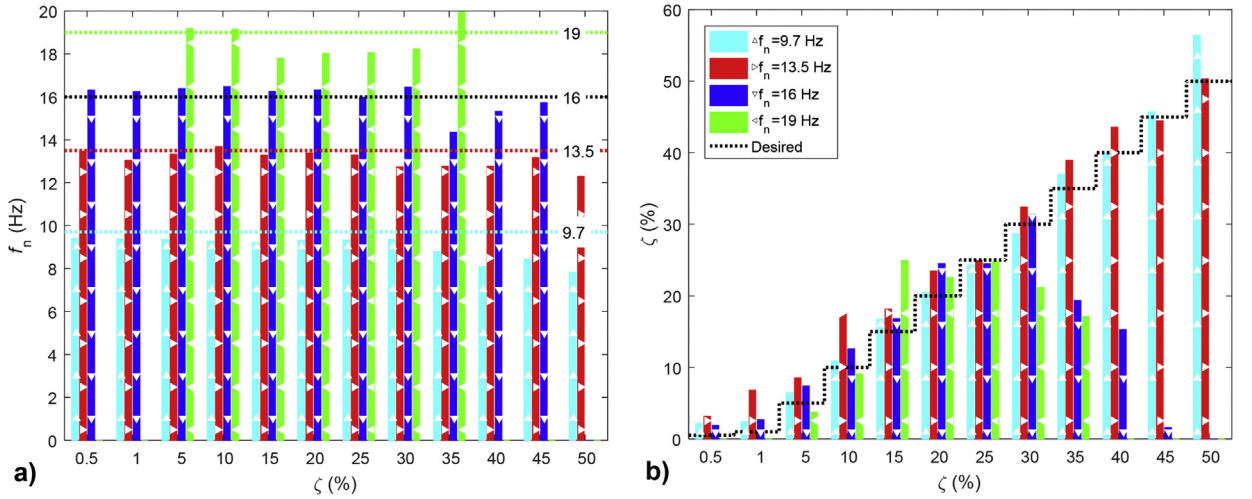

Fig. 13. Feedback linearisation, (a) measured natural frequencies and (b) measured damping ratios vs. assigned values.

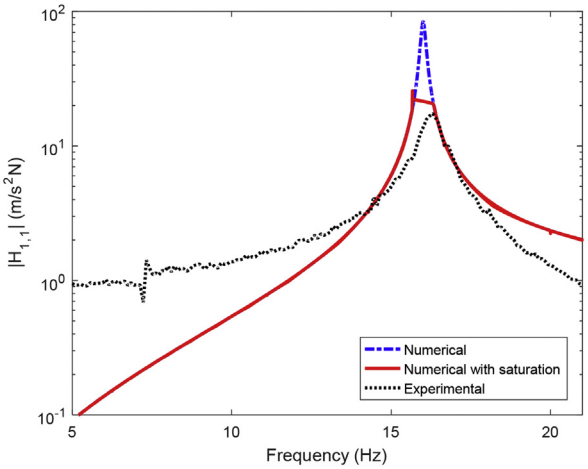

Fig. 14. Effect of the output saturation.

$$\zeta_n = \{0.5 \quad 1 \quad 5 \quad 10 \quad 15 \quad 20 \quad 25 \quad 30 \quad 35 \quad 40 \quad 45 \quad 50\}\%.$$

During all the tests, the nonlinear springs are known to act on the system until the motion decays to amplitudes lower than the gaps values. The experimental closed-loop FRFs of the linearised degree of freedom are shown in Fig. 11. It is seen that the controller is able to assign the desired dynamics in almost all cases. It completely cancels out the dynamics of the third mode, while a small part of the dynamics of the first mode at 6.9 Hz is not completely cancelled out but decreases when the desired natural frequency and damping ratio increases. The less than complete cancellation of the first mode is due to imperfections in the tuned model.

It is evident from Figs. 11 and 12 together that the experimental closed-loop FRFs match the numerical ones very closely. Similar to the experimental results, the simulated FRFs show the complete cancellation of the third mode while the first mode is less than completely cancelled especially in the FRFs with low damping. In this case, it is due to replication of experimental procedures by numerical differentiation of displacements to obtain velocities in the numerical model.

The response of the linearised system at low frequencies is seen to be higher in the numerical simulation than in the experiments due to the motion of the shaker in the low frequency range.

The natural frequencies and damping ratios of the closed-loop system were extracted using the PolyMAX algorithm and are compared to assigned values in Fig. 13. The closed-loop feedback linearisation is able to correctly apply the natural frequency and damping ratio in all cases, even though changing the natural frequency of a system by eigenvalue assignment is usually a very challenging task, even in linear systems. In the case in which only the damping ratio is different with respect to

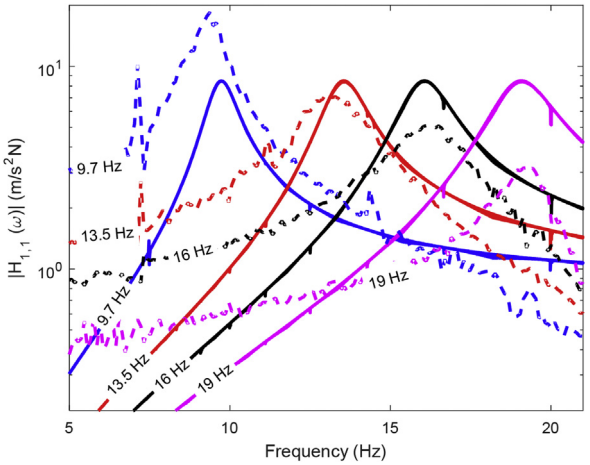

Fig. 15. Comparison between experimental (dashed line) and numerical (solid line) closed-loop FRFs for $\zeta_n = 5\%$.

the open loop system, i.e. $f_n = 9.7$ Hz denoted by the light blue bars in Fig. 13 (in the web version), the actual damping values are very well aligned with the desired ones, while the natural frequencies are slightly lower than expected. In the case of $f_n = 13.5$ Hz (red bars in Fig. 13 - in the web version) the experimental natural frequencies and damping ratios are all well aligned with assigned values. It is seen that the controller continues to assign natural frequencies and damping ratios very well until a certain level of damping ratio is reached, and from that point onwards the shaker begins to saturate and is unable to deliver the required control force. This effect becomes clear in Fig. 13 for the assigned natural frequency of 16 Hz (dark blue bars in Fig. 13 - in the web version) when the controller is able to assign the correct values of natural frequency and damping ratios until $\zeta_n = 30\%$. Thereafter, at higher assigned damping values, the natural frequencies are accurately assigned while the damping ratio results are consistently and increasingly lower than desired. At $\zeta_n = 50\%$ the eigenvalue is not identified. In the final case of an assigned natural frequency at 19 Hz, the same trend is evident in the damping ratios but saturation is reached at a lower value of damping because of the increased demand caused by shifting the natural frequency to an even higher value. The controller is not able to assign very low values of damping, less than 2%, probably because of internal damping in the shaker.

The result of numerical feedback linearisation, including force saturation, is provided in Fig. 14. Experimental and numerical FRFs both display the saturation effect of a truncated peak, which leads to an inaccurate estimate of the damping ratio.

A comparison between numerical and experimental FRFs for the four assigned natural frequencies with $\zeta_n = 5\%$ are shown in Fig. 15. The experimental trend is again very similar to the numerical one, but there are discrepancies in the vibration amplitude especially at low frequencies. The reason for this is that the numerical FRFs are obtained by swept-sine tests, while the experimental ones are determined from hammer tests. The closed-loop control is able to linearise the output and the FRFs are close to a single degree of freedom system. Also, the assigned natural frequencies are located exactly at the -90° phase point, as in Fig. 16, and the slope of the phase decreases with increasing the damping ratio. The experimental time domain response z_1 to the impact, in Fig. 17, shows a single harmonic response, which confirms that the linearised part of the partially linearised system is independent of the internal dynamics. The decay time of the response clearly decreases when the damping ratio is increased.

The FRFs of the internal dynamics with $\zeta_n = 5\%$ are shown in Fig. 18. The numerical internal dynamics FRF shows three major peaks: one corresponding to the assigned natural frequency, i.e. the effect of the linearised degree of freedom on the internal dynamics, and the other two related to resonances of the nonlinear internal dynamics. A jump due to the hardening effect can be seen in the second row of numerical FRFs $\mathbf{H}_{1,3}$, because the internal dynamics is nonlinear. The experimental results follow the same trend but do not catch the jump and show higher order harmonic components, due to the nonlinearity. The FRFs obtained with higher damping ratios (not shown) display very similar behaviour with the peak of the desired eigenvalue less visible when the damping ratio increases.

The time domain responses of the internal dynamics are shown in Fig. 19. The amplitude of the responses is much smaller than those of the linearised degree of freedom. The scales of z_3 and z_4 respectively in Fig. 19 are amplified by factors of two and four times that of the linearised degree of freedom z_1 in Fig. 16. It should be remembered that z_4 represents the displacement of the third mass. Thus in Fig. 19(b), when the gap size is superimposed on the time response, it is seen that approximately equal periods of time are spent with the gaps open and closed. The responses show a multi-harmonic behaviour as expected. The decay time is much longer than the decay time of the linearised degree of freedom but was found to be completely decayed at around 30 s.

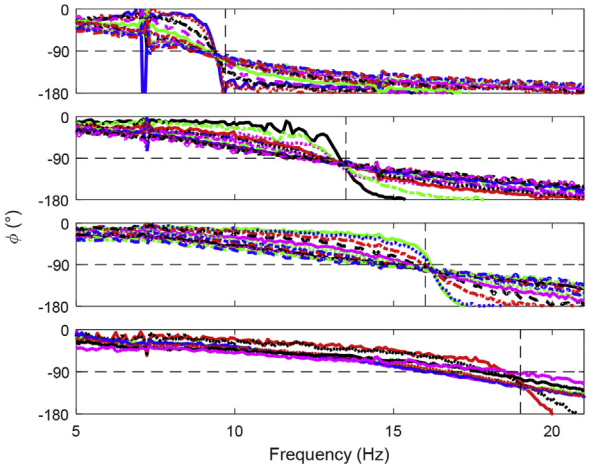

Fig. 16. Experimental closed loop FRF phases.

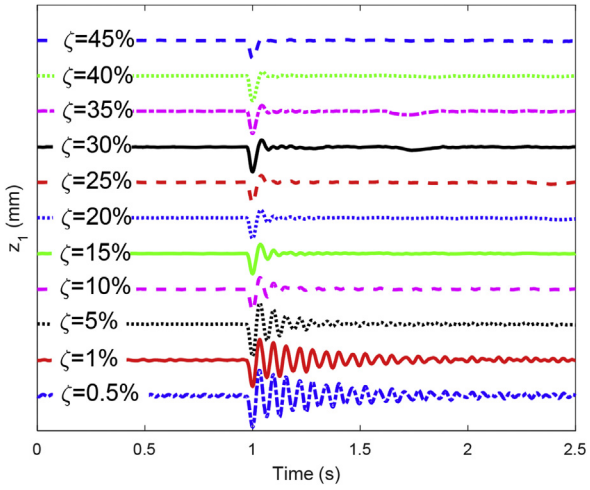

Fig. 17. Time domain z_1, $f_n = 16$ Hz.

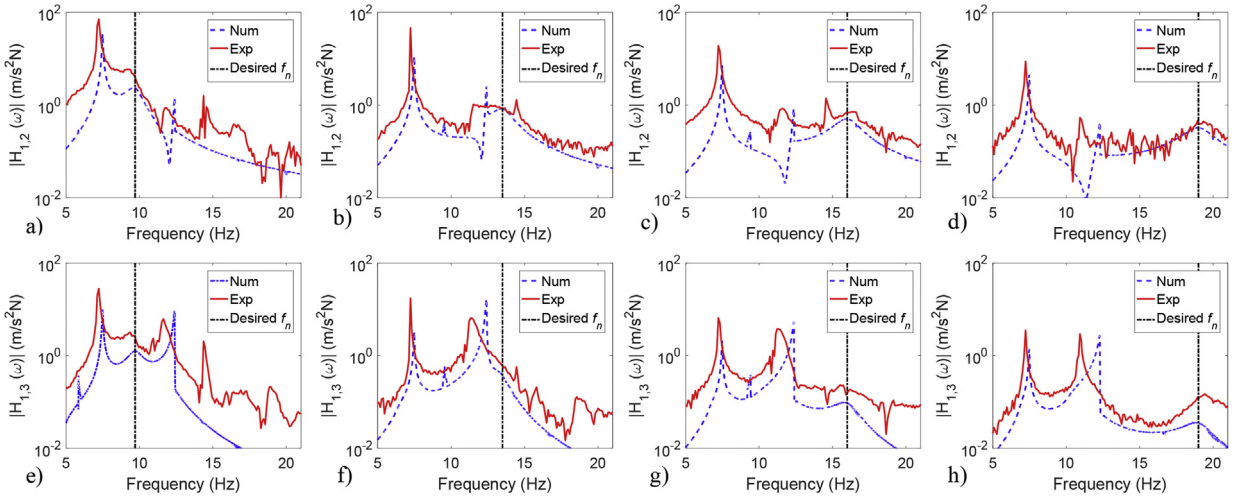

Fig. 18. Internal dynamics numerical and experimental closed loop FRFs for different values of natural frequency and $\zeta = 5\%$: (a)–(d) $|H_{1,2}|$, (e)–(h) $|H_{1,3}|$.

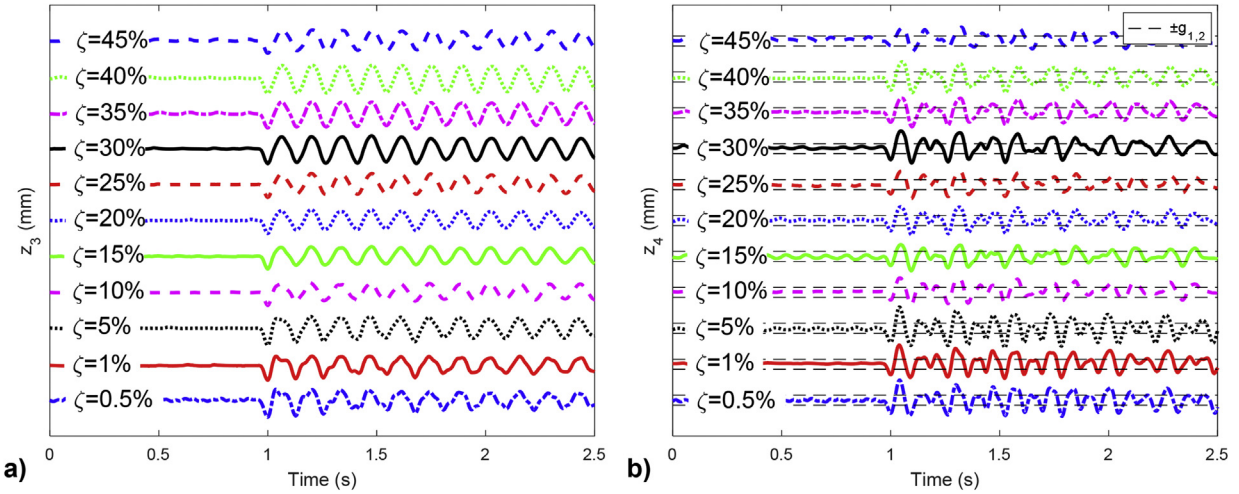

Fig. 19. Experimental time domain response of the internal dynamics $f_n = 16$ Hz and increasing values of damping: a) z_3 and b) z_4.

10. Conclusion

An experimental investigation of input-output partial feedback linearisation on a three degrees of freedom nonlinear system with piecewise linear stiffness is reported in this paper. The input and output share the same first degree of freedom while the nonlinearity is located at the third degree of freedom. This arrangement results in non-smooth, nonlinear zero dynamics that are shown to be stable, causing the entire system to be stable when the eigenvalues of the linearised part are positively damped. Successful partial feedback linearisation is achieved with the linearised first degree of freedom displaying a single mode - at the assigned original second natural frequency and above - while the other modes are almost completely cancelled out, except small effects caused by slight imperfections in the tuned model. The uncontrollable internal dynamics are shown to be stable with three main peaks and further nonlinear resonance effects. Excellent agreement is achieved between experimental and numerical results, except for saturation of the shaker which occurs when the assigned eigenvalues are too far away from the open-loop natural frequencies and damping ratios. The experiments described here validate the theory previously reported by two of the present authors.

Acknowledgements

The research described in this paper was carried out during a visit by the first author to the University of Liverpool. Mr Lisitano acknowledges the support of an Erasmus+ Traineeship funded by the European Commission.

Appendix A. Stability of the zero dynamics

The application of partial feedback linearisation requires stability of the zero dynamics for the overall stability of the system. A physical argument can be made in the present case to support the proposition that the system is stable. The piecewise-linear nature of the system means that if its displacement lies outside the central region $-g_1 < z_4 < g_2$, then it will be driven within that region when sufficient energy has been dissipated through damping. Once inside the central region the system is linear with a zero equilibrium state. However, for purposes of completeness a brief mathematical derivation will now be provided.

The zero dynamics of Eq. (19) may be written as,

$$\dot{\mathbf{z}}_{zd} = \mathbf{A}\mathbf{z}_{zd} + \mathbf{b}f_{nl} \tag{A.1}$$

with the obvious definition of matrix $\mathbf{A}$, vectors $\mathbf{b}$ and f_{nl}, and equilibrium points are found that satisfy,

$$\mathbf{A}\mathbf{z}_{eq} + \mathbf{b}f_{nl} = \mathbf{0} \tag{A.2}$$

The nonlinearity is piecewise linear, so that,

$$f_{\mathrm{nl}} = \begin{cases} k_2(z_4 - (-g_1)) & z_4 < -g_1 \\ 0 & -g_1 < z_4 < g_2 \\ k_2(z_4 - g_2) & z_4 > g_2 \end{cases} \tag{A.3}$$

Using the substitution $z_4 = \mathbf{e}_2^{\mathrm{T}}\mathbf{z}_{\mathrm{eq}}$ and $\mathbf{e}_2 = \mathbf{I}^{4\times 4}_{(:,2)}$,

$$f_{\mathrm{nl}} = \begin{cases} k_2\mathbf{e}_2^{\mathrm{T}}\mathbf{z}_{\mathrm{eq}} + k_2 g_1 & z_4 < -g_1 \\ 0 & -g_1 < z_4 < g_2 \\ k_2\mathbf{e}_2^{\mathrm{T}}\mathbf{z}_{\mathrm{eq}} - k_2 g_2 & z_4 > g_2 \end{cases} \tag{A.4}$$

The equilibrium point has to be found in each of the three regions. In the central region, $-g_1 < z_4 < g_2$, from Eq. (A.1) and Eq. (A.3),

$$\mathbf{A}\mathbf{z}_{\mathrm{eq}} = \mathbf{0} \tag{A.5}$$

Since $\mathbf{A}$ is full rank, then,

$$\mathbf{z}_{\mathrm{eq}} = \mathbf{0} \tag{A.6}$$

In the first outer region $z_4 < -g_1$, from Eq. (A.1) and Eq. (A.3),

$$\mathbf{A}\mathbf{z}_{\mathrm{eq}} + \mathbf{b}\left(k_2\mathbf{e}_2^{\mathrm{T}}\mathbf{z}_{\mathrm{eq}} + k_2 g_1\right) = \mathbf{0} \tag{A.7}$$

$$\mathbf{z}_{\mathrm{eq}} = -\left[\mathbf{A} + \mathbf{b}k_2\mathbf{e}_2^{\mathrm{T}}\right]^{-1}\mathbf{b}k_2 g_1 \tag{A.8}$$

This leads to,

$$\mathbf{z}_{\mathrm{eq}} = -\{\,0.0788 \quad 0.2606 \quad 0 \quad 0\,\}^{\mathrm{T}} g_1 \tag{A.9}$$

It is clear that $-0.2606 > -1$ and therefore there is no equilibrium point in the range $z_4 < -g_1$.

And the second outer region, $z_4 > g_2$, from Eq. (A.1) and Eq. (A.3),

$$\mathbf{A}\mathbf{z}_{\mathrm{eq}} + \mathbf{b}\left(k_2\mathbf{e}_2^{\mathrm{T}}\mathbf{z}_{\mathrm{eq}} - k_2 g_2\right) = \mathbf{0} \tag{A.10}$$

$$\mathbf{z}_{\mathrm{eq}} = \left[\mathbf{A} + \mathbf{b}k_2\mathbf{e}_2^{\mathrm{T}}\right]^{-1}\mathbf{b}k_2 g_2 \tag{A.11}$$

This leads to,

$$\mathbf{z}_{\mathrm{eq}} = \{\,0.0788 \quad 0.2606 \quad 0 \quad 0\,\}^{\mathrm{T}} g_2 \tag{A.12}$$

It is clear that $0.2606 < 1$ and therefore there is no equilibrium point in the range $z_4 > g_2$.

The stability of each of the three equilibrium points in each of the three ranges was investigated in detail by the present authors [22]. They discovered theoretically and in numerous simulations that the two non-zero equilibria were stable only in case of zero stiffness in the central region (i.e. freeplay). Otherwise, as in the present case, the two non-zero equilibria were found to be points of neutral stability.

Thus, the only equilibrium point to be considered is $\mathbf{z}_{\mathrm{eq}} = \mathbf{0}$ and, since the zero dynamics are non-smooth, its stability will be analysed with a general Lyapunov approach for non-smooth systems [27],

$$V = \frac{1}{2}\mathbf{z}_{\mathrm{zd}}\mathbf{P}\mathbf{z}_{\mathrm{zd}}, \quad \mathbf{P} > 0, \quad \mathbf{P}^{\mathrm{T}} = \mathbf{P} \tag{A.13}$$

It may be shown using the calculus of the Filippov differential inclusion [28], applied in non-smooth feedback linearisation in Ref. [22], that

$$\dot{V} = \mathbf{z}_{\mathrm{zd}}^{\mathrm{T}}\mathbf{P}(\mathbf{A}\mathbf{z}_{\mathrm{zd}} + \mathbf{b}f_{\mathrm{nl}}) \tag{A.14}$$

which in the three regions can expressed as,

$$\dot{V} = \begin{cases} \mathbf{z}_{zd}^{T}\mathbf{P}(\mathbf{A}\mathbf{z}_{zd} + \mathbf{b}\{k_2[z_4 - (-g_1)] + \varepsilon\,\mathrm{sgn}(z_6)|k_2[z_4 - (-g_1)]|\}) \\ \mathbf{z}_{zd}^{T}\mathbf{P}\mathbf{A}\mathbf{z}_{zd} \\ \mathbf{z}_{zd}^{T}\mathbf{P}(\mathbf{A}\mathbf{z}_{zd} + \mathbf{b}[k_2(z_3 - g_2) + \varepsilon\,\mathrm{sgn}(z_6)|k_2(z_3 - g_2)|]) \end{cases} \tag{A.15}$$

Therefore, stability is governed by the negative definiteness of each of the three expressions in Eq. (A.15), and inside the central region by,

$$\mathbf{P}\mathbf{A} \prec 0 \tag{A.16}$$

Since a matrix $\mathbf{P}$ can always be found to satisfy Eq. (A.16) the system is found to have a stable zero equilibrium.

Appendix B. Partial feedback linearisation applied to SISO lumped mass systems

A sufficient condition for partial feedback linearisation is that input appears explicitly after differentiating the output a finite number times, known as the relative degree and denoted by n.

For reasons of simplicity a single-input single-output (SISO) will be considered. Then, without loss of generality an N degree of freedom lumped mass system with input at the first coordinate may be chosen. The output is assumed to be at the χ^{th} coordinate and the non-smooth nonlinearity at the η^{th} coordinate.

Using the nomenclature introduced in §6 the expression for the state space model may be re-written as,

$$\mathbf{f}(x) = \begin{Bmatrix} \mathbf{x}_{N+1:2N} \\ -\mathbf{M}^{-1}(\mathbf{K}\mathbf{x}_{1:N} + \mathbf{C}\mathbf{x}_{N+1:2N} + \mathbf{f}_{nl}) \end{Bmatrix}; \quad (f_{nl})_{\eta} \neq 0 \tag{B.1}$$

and,

$$\mathbf{g}(x) = \begin{Bmatrix} \mathbf{0}_{N\times 1} \\ \mathbf{M}^{-1}\mathbf{g}_q \end{Bmatrix}; \quad \mathbf{M}^{-1} = \begin{bmatrix} {}^{1}/_{m_{11}} & & & \\ & {}^{1}/_{m_{22}} & & \\ & & \ddots & \\ & & & {}^{1}/_{m_{NN}} \end{bmatrix}; \quad \mathbf{g}_q = \begin{pmatrix} 1 \\ 0 \\ \vdots \\ 0 \end{pmatrix}_{N\times 1} \tag{B.2}$$

Thus,

$$g_j(x) = 0; \quad g_{j=N+1}(x) = 1/m_{11}; \quad j = 1, \ldots, 2N \tag{B.3}$$

The presence of the input in the ith derivative of the output depends upon the nonzero entries of the term $\mathbf{g}(x) \in \Re^{2N\times 1}$.

Then, by carrying out differentiation of the output,

$$z_1 = y = x_{\chi=1} \tag{B.4}$$

$$z_2 = \dot{z}_1 = \ddot{y} = \dot{x}_{\chi=1} = x_{N+\chi=N+1} \tag{B.5}$$

$$z_3 = \dot{z}_2 = \ddot{z}_1 = \dddot{y} = \dot{x}_{N+\chi=N+1} = f_{N+\chi=N+1}(x) + g_{N+\chi=N+1}(x) \times u(t) \tag{B.6}$$

Therefore a transformation matrix can be formed between linear and nonlinear coordinate systems and the first coordinate can be linearised as in §6.

If the degree of freedom of the output is different from the degree of freedom of the input $(\chi \neq 1)$, then

$$z_1 = y = x_{\chi} \tag{B.7}$$

$$z_2 = \dot{z}_1 = \ddot{y} = \dot{x}_{\chi} = x_{N+\chi} \tag{B.8}$$

$$z_3 = \dot{z}_2 = \ddot{z}_1 = \dddot{y} = \dot{x}_{N+\chi} = f_{N+\chi}(x) + g_{N+\chi}(x) \times u(t) = f_{N+\chi}(x) \tag{B.9}$$

because $g_{N+\chi}(x) = 0$.

$$z_4 = \dot{z}_3 = \frac{\partial}{\partial t}\left(f_{N+\chi}(x)\right) = \frac{\partial}{\partial t}\left(-\frac{1}{m_{\chi\chi}}\left(\mathbf{K}_{\chi,1:N}\mathbf{x} + \mathbf{C}_{\chi,1:N}\dot{\mathbf{x}}\right)\right) + \frac{\partial}{\partial t}\left(-\frac{1}{m_{\chi\chi}}f_{\mathrm{nl}_\chi}\right) \tag{B.10}$$

If $\chi = \eta$ differentiation of the nonlinear term is required and therefore feedback linearisation is not feasible. If $\chi \neq \eta$, then in principle differentiation can continue but the transformation matrix is found not to allow the required separation of the linearised subsystem from the nonlinear internal dynamics, and therefore, once again, feedback linearisation is found not to be feasible. This observation can be readily tested on simulated examples and extends to the case of multiple-input multiple-output partial feedback linearisation.

Therefore, in a lumped-mass system, with no inertial coupling, it is necessary to have the input at the same degrees of freedom as the output for partial feedback linearisation.

Appendix C. Control of the input force

Outer loop control is not effective because the force provided by the shaker is directly proportional to the current in the electromagnetic coils and not the output voltage from dSPACE. Therefore an inner PD controller is necessary to regulate the shaker force in real time. In this case the proportional and derivative coefficients of the controller were tuned manually to reproduce sine waves in the range of interest from 4 to 21 Hz. The three natural frequencies of the system and the assigned frequencies were all within this range and it was found that the resulting controller was able to deliver the inputs commanded by outer-loop linearising controller with good accuracy as shown in Figs. C.1 and C.2. The output of the PD controller is a voltage to drive the shaker and is subject to a saturation term in dSPACE to ensure the safety of the hardware.

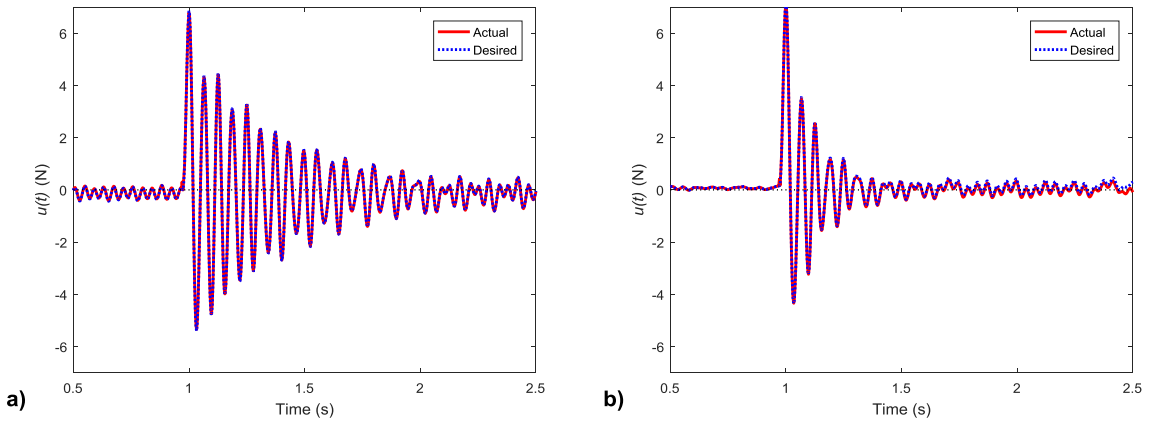

Fig. C.1. Commanded and achieved input for $f_n = 16$ Hz: a) $\zeta_n = 0.5\%$ and b) $\zeta_n = 5\%$.

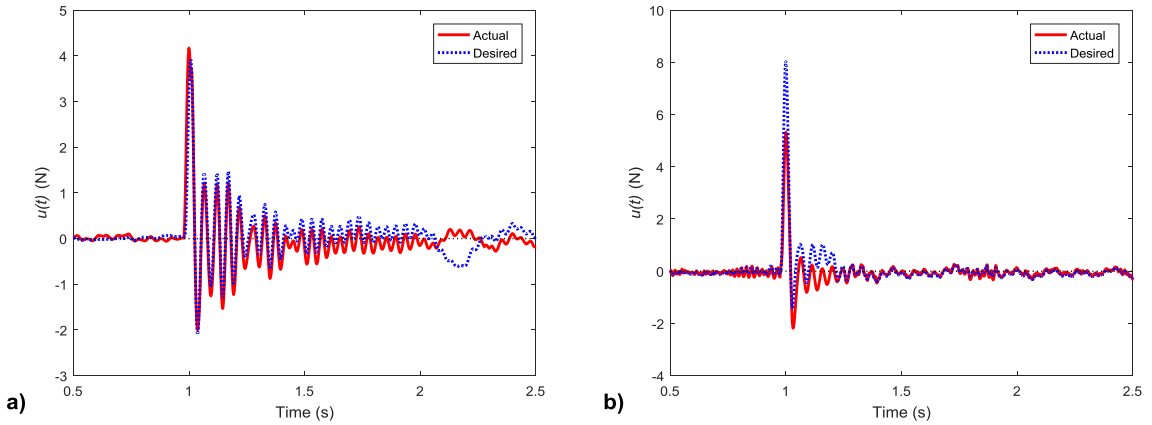

Fig. C.2. Commanded and achieved input for $f_n = 19$ Hz: a) $\zeta_n = 5\%$ and b) $\zeta_n = 35\%$.

The figures show typical command signals from the outer-loop feedback linearising controller and achieved force inputs, the latter being measured by the load cell and provided to the system. The system is initially at rest and excitation is delivered at t = 1 s with the controller switched on. In Fig. C.1 the actual input reproduces the command signal very well, measured modal parameters are very close to the assigned ones and partial feedback linearisation is successfully applied. In Fig. C.2 the physical input is slightly different from the assigned one and, in the case of low damping (Fig. C.2(a)), the discrepancy is

acceptable and the controller is still able to assign the correct modal parameters. When the assigned damping is high (Fig. C2(b)) the discrepancy between actual and desired input becomes evident, due to the voltage saturation, and the controller is no longer effective in assigning the desired damping.

References

[1] A. Isidori, Nonlinear Control Systems, Springer, London, 1995.
[2] H.K. Khalil, Nonlinear Systems, Prentice Hall, New Jersey, 2002.
[3] M. Vidyasagar, Nonlinear System Analysis, Prentice Hall, New Jersey, 1993.
[4] B. d'Andrèa-Novel, G. Bastin, G. Campion, Dynamic feedback linearisation of nonholonomic wheeled mobile robots, in: Proc. of IEEE, Nice, France, 1992, pp. 2527–2532.
[5] A. De Luca, P. Lucibello, A general algorithm for dynamic feedback linearisation of robots with elastic joints, in: Proc. of IEEE, Leuven, Belgium, 1998, pp. 504–510.
[6] G. Oriolo, A. De Luca, M. Vendittelli, WMR control via dynamic feedback linearisation: design, implementation, and experimental validation, IEEE Trans. Control Syst. Technol. 10 (6) (2002) 835–852.
[7] B. d'Andrèa-Novel, G. Campion, G. Bastin, Control of nonholonomic wheeled mobile robots by state feedback linearisation, Int. J. Robotics Res. 14 (6) (1995) 543–559.
[8] F. Piltan, H. Rezaie, B. Boroomand, A. Jahed, Design robust backstepping on-line tuning feedback linearisation control applied to IC engine, Int. J. Adv. Sci. Technol. 43 (2012) 127–142.
[9] W. Mielczarski, A.M. Zajaczkowski, Nonlinear field voltage control of a synchronous generator using feedback linearisation, Automatica 30 (10) (1994) 1625–1630.
[10] J. Chiasson, Dynamic feedback linearisation of the induction motor, IEEE Trans. Autom. Control 38 (10) (1993) 1588–1594.
[11] O. Akhrif, F. Okou, L. Dessaint, R. Champagne, Application of a multivariable feedback linearisation scheme for rotor angle stability and voltage regulation of power systems, IEEE Trans. Power Syst. 14 (2) (1999) 620–628.
[12] T. Boukas, T. Habetler, High-performance induction motor speed control using exact feedback linearisation with state and state derivative feedback, IEEE Trans. Power Electron. 19 (4) (2004) 1022–1028.
[13] W. Na, B. Gou, Feedback-linearisation-based nonlinear control for PEM fuel cells, IEEE Trans. Energy Convers. 23 (1) (2008) 179–190.
[14] T. Kimura, S. Hara, T. Fujita, T. Kagawa, Feedback linearisation for pneumatic actuator systems with static friction, Control. Eng. Pract. 5 (10) (1997) 1385–1394.
[15] G. Vossoughi, M. Donath, Dynamic feedback linearisation for electrohydraulically actuated control systems, Trans. ASME 177 (1995) 468–477.
[16] A. Mokhtaril, A. Benallegue, B. Daachi, Robust feedback linearisation and GH controller for a quadrotor unmanned aerial vehicle, IEEE/RSJ Int. Conf. Intell. Robots Syst (2005) 1009–1014.
[17] D. Lee, J. Kim, S. Sastry, Feedback linearisation vs. adaptive sliding mode control for a quadrotor helicopter, Int. J. Control Autom. Syst. 7 (3) (2009) 419–428.
[18] S. Jiffri, P. Paoletti, J.E. Cooper, J.E. Mottershead, Feedback linearisation for nonlinear vibration problems, Shock Vib. (2014) 16. Article ID 106531.
[19] J. Ko, A.J. Kurdila, T.W. Strganac, Nonlinear control of a prototypical wing section with torsional nonlinearity, J. Guid. Control Dyn. 20 (6) (1997) 1181–1189.
[20] S. Jiffri, S. Fichera, J.E. Mottershead, A. Da Ronch, Experimental nonlinear control for flutter suppression in a nonlinear aeroelastic system, J. of Guidance, Control Dyn. (2017) 1925–1938. https://doi.org/10.2514/1.G002519.
[21] G. Tao, P. Kokotovic, Adaptive control of systems with unknown non-smooth non-linearities, Int. J. Adapt. Control Signal Process. 11 (1997) 81–100.
[22] S. Jiffri, P. Paoletti, J.E. Mottershead, Feedback linearisation in systems with non-smooth nonlinearities, J. Guid. Control Dyn. 39 (4) (2016) 814–825.
[23] D. Lisitano, C. Zhen, S. Jiffri, E. Bonisoli, J.E. Mottershead, An example of feedback linearization in a non-smooth system, in: Int. Conf. on Structural Eng. Dynamics, Ericeira, Portugal, 2017. Paper N. 030.
[24] B. Peeters, H. Van der Auweraer, P. Giullaume, J. Leuridan, The PolyMAX frequency-domain method: a new standard for modal parameter estimation? Shock Vib. 2004 (2004) 395–409.
[25] L.N. de Casto, J. Timmis, An artificial immune network for multimodal function optimisation, Evol. Comp. (2002) 699–704. CEC' 02 Proc. of the 2002 Congress, Honolulu, HI (2002).
[26] D. Cloutier, P. Avitabile, R. Bono, M. Peres, Shaker/stinger effects on measured frequency response functions, in: Proc. of the 27th IMAC, Orlando, Florida, 2009.
[27] D. Shevitz, B. Paden, Lyapunov stability theory of nonsmooth systems, IEEE Trans. Automat. Control 39 (9) (1994) 1910–1914.
[28] B.E. Paden, S.S. Sastry, A calculus for computing Filippov differential inclusion with application to the variable structure control of robot manipulators, IEEE Trans. Circuits Syst 34 (1) (1987) 73–82.